Spatiotemporal oscillations and clustering in the Ziff-Gulari-Barshad model with surface reconstruction

A. Provata[1] and V. K. Noussiou[1,2]
[1]*Institute of Physical Chemistry, National Center for Scientific Research "Demokritos," 15310 Athens, Greece*
[2]*Department of Chemistry, University of Athens, 10679 Athens, Greece*
(Received 7 June 2005; published 8 December 2005)

We study the dynamics of the Ziff-Gulari-Barshad (ZGB) model on square (sq) and hexagonal-honeycomb (hex) lattices and when surface restructuring is introduced. We show that the ZGB model exhibits nonequilibrium phase transitions on the hex lattice similar to the ones already observed on the sq lattice, but the critical values of the kinetic parameters depend crucially on the substrate type. If surface reconstruction (sq$\leftrightarrow$hex) is assumed for high lattice coverage of one of the reactive species then persistent spatiotemporal oscillations and clustering of homologous species are observed for kinetic parameter values $0.348 < k_1 < 0.393$.

DOI: 10.1103/PhysRevE.72.066108 PACS number(s): 82.40.Np, 05.10.Ln, 82.20.Wt

I. INTRODUCTION

One of the most technologically important heterogeneous catalytic reactions, the oxidation of carbon monoxide on catalytic substrates, has been identified as proceeding according to the Langmuir-Hinshelwood (LH) mechanism, or monomer-dimer reaction, described by the following steps:

$$[A_g] + * \xrightarrow{k_1} A_{ads}, \tag{1a}$$

$$[B_{2,g}] + 2* \xrightarrow{1-k_1} 2B_{ads}, \tag{1b}$$

$$A_{ads} + B_{ads} \xrightarrow{k_2} 2* + [AB_g]. \tag{1c}$$

The index *ads* refers to species adsorbed on catalytic sites and *g* refers to species at the gaseous phase above the catalytic surface. In the particular case of CO oxidation, the species *A* represents CO, *B* represents O, and $*$ denotes the empty catalytic sites. Over the past decades numerous experimental studies on heterogeneously catalyzed reactions, including CO oxidation, have demonstrated sustained temporal oscillations at the steady state and pattern formation at the mesoscale [1–11]. In parallel, many theoretical and numerical models were developed, in order to clarify the basic mechanisms responsible for the development of these features [11–22].

In a celebrated paper in 1986, Ziff, Gulari, and Barshad (ZGB) proposed a model in which the catalytic support is represented by a square lattice and the reactive dynamics is represented by a lattice gas type of process. This model is called the standard ZGB model [14]. The basic assumptions of the ZGB model are that (a) the lattice or surface is in contact with a mixture of *A* (CO) and B_2 (O_2) in the gaseous phase, (b) the relative concentrations of the two gases determine the kinetic rates at which they adsorb on the empty lattice sites, (c) *A* (CO) adsorbs on one empty site, (d) B_2 (O_2) adsorbs dissociatively on two adjacent empty sites, (e) the adsorbed species are diffusionless, and (f) if *A* (CO) and *B* (O) are placed on nearest neighbor (NN) sites they immediately react. In the parameter space this model predicts two kinetic phase transitions which define three states in the phase space, an O poisoned state for $0 \leqslant k_1 = y_{CO} \leqslant 0.389$, $k_2 = 1.0$, a CO poisoned state for $0.525 \leqslant k_1 = y_{CO} \leqslant 1$, $k_2 = 1.0$ (where y_{CO} is the mole fraction of CO in the gas phase), and a reactive state between these two transition points with coexistence of CO and O on the catalytic surface.

The ZGB model successfully predicted the poisoning transitions that take place on single crystal catalysts such as perfect Pt(100), but has neglected, for reasons of simplicity, important phenomena, such as diffusion of the reactive species on the lattice, desorption of the reactants, reactant intrusion to layers below the surface, surface restructuring, etc. All or some of these events may take place depending on the experimental conditions, temperature, gas partial pressures, and surface coverages. As a result of neglecting these phenomena, some experimentally observed notorious features of the CO oxidation (and other catalytic reactions) are not predicted by the standard ZGB model. These unpredicted features include sustained kinetic oscillations of the lattice coverages, pattern formation at the mesoscale, cellular structures, wave front propagation, spirals, stripes, etc. [1–9].

A number of modifications to the standard ZGB model have revealed more complex dynamics bringing the model closer to experiments. If surface diffusion of the reactants is added to the model the transition points are shifted [15]. Long range repulsions (the "eight-site rule") of O_{ads} in addition to diffusion and superlattice ordering cause bistability and the order-disorder transition [16]. Further modifications include the "hybrid model" which assumes mean-field type behavior for infinitely mobile CO and lattice gas treatment for immobile O [17]. Introducing the formation of surface oxide to the ZGB mechanisms complicates the kinetics and is shown to modify the reaction rates by several orders of magnitude [18].

From experimental studies it is shown that surface reconstruction takes place under certain experimental conditions and, as a result, temporal oscillations of the partial surface coverages emerge. To understand the interplay between surface restructuring and oscillations mean-field models are proposed, which use variables representing the surface structure (e.g., hexagonal vs square) coupled with variables represent-

ing the surface concentrations [19]. More recently, numerical Monte Carlo simulations and lattice gas cellular automata models, which address the mesoscopic mechanisms producing these oscillations, have been proposed. Zhdanov and coworkers [20] have used a two-layer representation of the Pt(110) surface with surface reconstruction based on different energetics (attractive and repulsive depending on the direction) and have demonstrated oscillation of the surface partial coverages. A lattice gas cellular automaton model was also used by Kapral and co-workers [21] to model the CO oxidation on metallic surfaces. This model is based on multiple occupancy of the cells (several different species may reside on the same spatial point), in which the $(\text{hex}) \leftrightarrow (1 \times 1)$ local transitions are introduced through a number of rules depending dynamically on the local environment while the kinetic constants and other parameters are different in the hex and (1×1) configurations.

Due to its minimalistic character the original ZGB model has not taken into account surface reconstruction phenomena and although the direct presence of a substrate surface gives rise to steady state, concentration phase transitions, temporal oscillatory phenomena are not observed. A ZGB variant mechanism leading to global oscillations is proposed by Kortlüke *et al.* [22] where each lattice site is found either in the hex $\equiv \alpha$ phase or in the unreconstructed $(1 \times 1) \equiv \beta$ phase of the Pt(100) surface [and similarly for the Pt(110) surface]. The $\alpha \leftrightarrow \beta$ transition of a site happens at the borders between α and β phases depending on the CO local occupation and this induces transient oscillations. If, in addition, a weak noise is induced via a spontaneous $\alpha \leftrightarrow \beta$ transition, independently of the local environment, this noise amplifies the synchronization and leads to global oscillations.

In the current study a minimal complexity mechanism with naturally emerging oscillations due to surface reconstruction is presented. The proposed model does not simulate realistic experimental conditions but addresses basic mechanisms coupling sustained oscillations with surface restructuring. The central idea is to perform direct lattice reconstruction in parallel with reacting events via kinetic Monte Carlo (KMC) simulations [23]. This direct lattice restructuring seems to be responsible for the development of sustained temporal concentration oscillations at the steady state as is observed in experiments. To achieve this we follow a step-by-step procedure.

In the next section we first choose to characterize the kinetics of the LH mechanism via KMC simulations on purely hexagonal-honeycomb (hex) lattice and compare it with the kinetics on the purely square (sq) lattice. As we will see, the results are qualitatively the same, but quantitatively the parameter values where the kinetic phase transitions take place are shifted. In Sec. III we perform KMC simulations on a lattice which changes configuration from sq to hex and back depending on the instantaneous concentrations (the kinetic parameters do not change in the $\text{sq} \leftrightarrow \text{hex}$ transition; only the number of bonds changes). This combined mechanism leads to sustained temporal oscillations of the surface coverage which occur at certain parameter zones. In Sec. IV we study the dynamics of clustering when surface reconstruction takes place and in the concluding section we recapitulate our main results and discuss open problems.

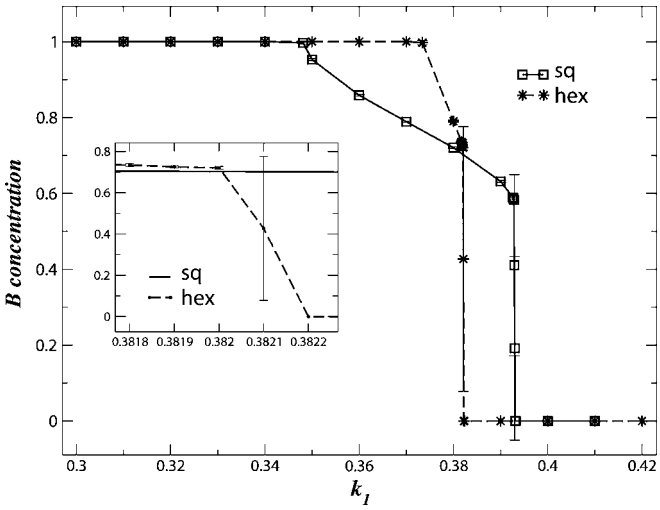

FIG. 1. The average steady state concentration of B for hex (stars) and sq (squares) lattice configurations.

II. THE ZIFF-GULARI-BARSHAD MODEL ON SQ AND HEX LATTICES

The algorithm variant introduced here for the description of the LH monomer-dimer mechanism is slightly different from the standard ZGB algorithm mainly in taking into account delays in the formation of the AB ($\equiv CO_2$) complex and subsequent desorption. The algorithm is the same for sq and hex lattices and is described by the following steps.

(1) Start with an empty lattice containing N sites.

(2) For every elementary time step (ETS) choose one lattice site at random and a random number r, $0 \leqslant r \leqslant 1$, that determines which reaction will take place.

(3) If the chosen lattice site is empty and $r \leqslant k_1$ then one A particle is adsorbed on the chosen site.

(4) If the chosen lattice site is empty and $r \geqslant k_1$ and a randomly selected nearest neighbor is also empty then B_2 is adsorbed dissociatively on the chosen site and NN.

(5) If the chosen site contains an A (B) particle, a randomly selected neighbor contains a B (A) particle and $r \leqslant k_2$ then an AB complex is formed and desorbs immediately.

(6) In all other cases the lattice state remains unchanged.

(7) One ETS is completed and the algorithm returns to step 2 for a new ETS to start.

(8) One Monte Carlo step (MCS) is completed after a number of ETSs equal to the total number of lattice sites. In one MCS each lattice site has reacted once on average.

The difference between the above algorithm and the standard ZGB is that step (1c) reaction-desorption does not take place instantly but A and B may spend some time on nearest neighboring lattice sites before they are selected to form the AB complex and desorb. This modification only shifts the boundaries of the reactive zone with respect to the standard ZGB model and does not induce qualitative changes. In the remaining of the work the value of k_2 fixed to 1.0, for simplicity.

In Fig. 1 we present the steady state concentrations of B as a function of k_1. The lattice substrate contains in total

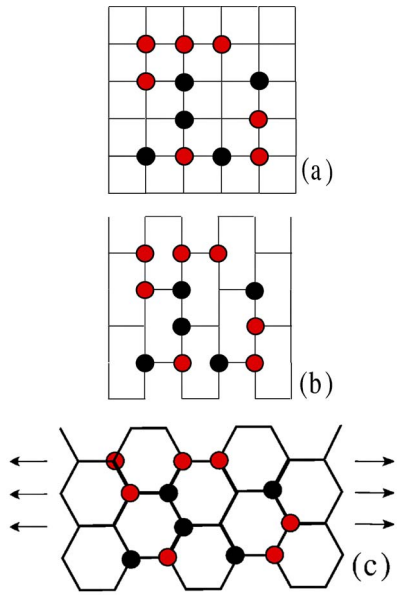

FIG. 2. (Color online) Surface reconstruction process: (a) square lattice, (b) intermediate "brick-wall" lattice, and (c) hexagonal-honeycomb lattice. The black and gray (red) spheres represent A and B particles, respectively.

25×10^4 sites, for both the hex and sq configurations. Results represent averages over ten KMC runs. In both cases we observe one smooth and one abrupt phase transition as in [14]. The transition points are for the sq lattice 0.3481 and 0.3930, while for the hex lattice 0.3734 and 0.3821. Uncertainties of these values are of the order of 2×10^{-4}. The inset in Fig. 1 magnifies the abrupt hex transition region and shows that the error bars there are of the order of the gap size. Away from the abrupt transition the errorbars are of the order of the symbol sizes or smaller and they are visible within the open symbols (squares). The reason for the different quantitative behavior between the hex and sq configurations in the intermediate k_1-value zone is the different number of NNs (three NNs in the hex configuration and four NNs in the sq configuration). The variation in the number of NNs is important in the occurrence of synergetic steps (1b) and (1c) which are, thus, more frequently realised in the sq than in the hex configuration.

When combining the hex and sq cases we expect to observe spatiotemporal oscillatory dynamics in the parameter zone $0.3481\leqslant k_1<0.3930$ (called the R zone) where the square and hex configurations lead to different steady states.

III. SURFACE RECONSTRUCTION

To perform the surface reconstruction we modify our algorithm by adding the following steps inside the algorithm.

(9) After every MCS the global coverage by particles B, b, is calculated.

(10) If the lattice is in the hex (sq) configuration and b is less (greater) than a lower (upper) cutoff then some NN links are added (removed) as shown in Fig. 2. (The cutoffs are comparable with the steady state b values for the given parameters). Now each lattice site has four (three) NN links and the configuration corresponds to perfect sq (hex) lattice as indicated in Figs. 2(a) and 2(c).

Note that the kinetic parameters do not change when going from sq$\leftrightarrow$hex configurations, only the number of bonds change, as can be seen in Fig. 2.

Representative temporal evolution of the system in the R zone is presented in Fig. 3. Sustained oscillations of the B occupation and the $AB_{(gas)}$ production are observed for $k_1=0.385$, and similar behavior is obtained for the occupation of A particles and vacant sites. The linear lattice size used is $L=100$ which corresponds to 10^4 substrate sites. Similar sustained oscillations are observed for all parameter values in the R zone, since within this region we have a discrepancy between the steady state value in the square and the hex configuration. Oscillations are more prominent for

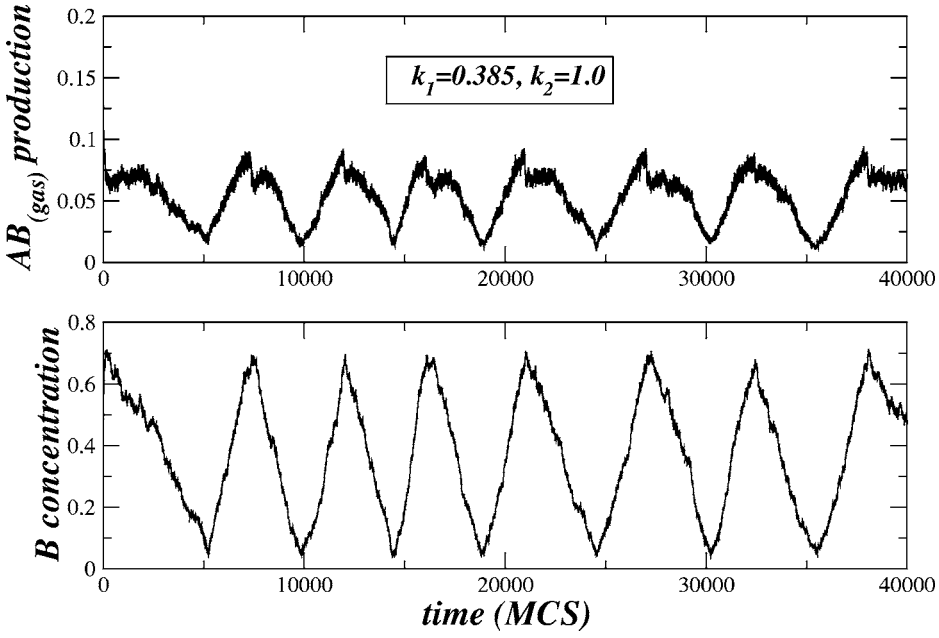

FIG. 3. Temporal oscillations of B and the persite AB_{gas} production rate observed when the system undergoes lattice phase transitions between sq and hex configurations. The lattice size is $L=100$ and the kinetic constants are $k_1=0.385$ and $k_2=1.0$.

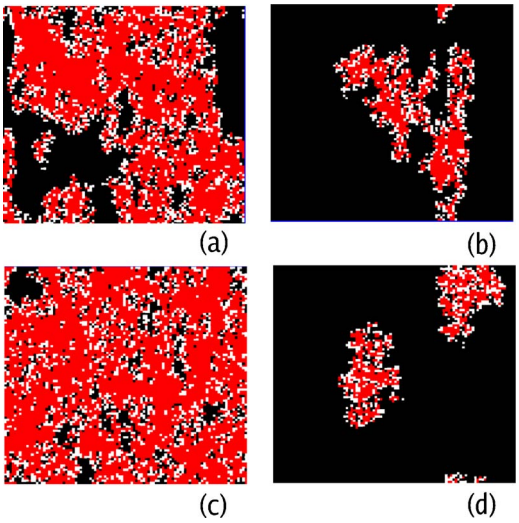

FIG. 4. (Color online) Detailed lattice snapshots taken at times (a)2500, (b) 5000, (c) 7500, and (d) 10 000 MCSs. The lattice size is $L=100$ and the kinetic constants are $k_1=0.385$ and $k_2=1.0$.

$k_1>0.3821$ since the concentration gaps in the hex and sq phases are larger as compared to the case $k_1<0.3821$. When there is an important difference in the steady state concentrations, oscillations are not blurred by noise. Note that for $k_1=0.3821$, both sq and hex configurations lead to similar results.

The mechanism producing the oscillations is understood as follows. Initially the system is in the hex configuration. In this state there are only three links for each site and thus synergetic steps (1b) and (1c) are not favoured but happen with low probability. Step (1a) is favored since it takes place spontaneously and thus the partial lattice concentration of A grows while the B and $*$ concentrations remain small. When the concentration of B achieves an upper threshold value (of the order of 0.65 for Fig. 3) then a phase transition occurs and the lattice assumes the hex configuration. Maximum A (minimum B) concentration occurs at the end of the hex phase. In the sq configuration each site has four nearest neighbors and steps (1b) and (1c) are facilitated, while the situation does not change for step (1a). Due to the large values of the kinetic constants in steps (1b) and (1c) (0.6 and 1.00, respectively) the concentration of A decreases due to desorption (1c) while the concentration of B increases due to adsorption (1b). The system then achieves a state with high B and low A concentration and the lattice changes back from sq to hex configuration and a new cycle starts.

Representative snapshots of the spatial coverages are shown in Fig. 4. In Fig. 4(a) the system in the hex configuration accumulates B [red (gray)] particles while A (black) regions start forming. In Fig. 4(b) the system is toward the end of the hex phase with extended A (black) regions. In Fig. 4(c) the system is toward the end of the sq phase and has accumulated many B (red) particles. Fig. 4(d) shows similar features as Fig. 4(b). The lattice size in Fig. 4 is $L=100$ and the kinetic constants are $k_1=0.385$ and $k_2=1.0$, as in Fig. 3.

IV. CLUSTERING

Due to the cooperative character of steps (1b) and (1c) cluster formation is expected (and observed) in the system [24]. To calculate the degree of cluster formation during the temporal evolution of the system a variable $l(i,j)$ is defined on every site (i,j) of the lattice, taking the values

$$l(i,j)=\begin{cases}1 & \text{if site } (i,j) \text{ is covered by particles } A,\\ -1 & \text{if site } (i,j) \text{ is covered by particles } B,\\ 0 & \text{if site } (i,j) \text{ is empty.}\end{cases} \tag{2}$$

The degree of clustering is calculated via the temporal covariance function $C(t)$ defined as

$$C(t)=\frac{1}{2L^2}\sum_{i,j=1}^{L}\{[l(i,j)-l_{av}(t)][l(i+1,j)-l_{av}(t)] + [l(i,j)-l_{av}(t)][l(i,j+1)-l_{av}(t)]\} \tag{3}$$

where $l_{av}(t)$ denotes the time dependent average value of the variable $l(i,j)$ over the entire lattice. The function $C(t)$ takes the value 0 for a random, noncorrelated distribution of the variable l, and takes positive values if clustering occurs.

In Fig. 5 the temporal dependence of $C(t)$ is depicted corresponding to the oscillations shown in Fig. 3. The lattice size used is $L=100$ and the kinetic constants are $k_1=0.385$ and $k_2=1.0$, as in Figs. 3 and 4. It is evident that during one circle of oscillations there are two peaks in $C(t)$, one which demonstrates principally clustering of A and occurs during the hex phase and a second one which represents clustering of B and occurs during the sq phase. Clustering of A and B regions occurs due to the cooperative steps (1b) and (1c). In particular, step (1c) occurs in border regions between A and B clusters. As a result of this reaction two sites are liberated. In these empty sites either two B particles will be deposited dissociatively and thus the B cluster will grow at the expense of A, or one A will be deposited and one empty site will remain. In the remaining single empty site most probably another A will be deposited in a later ETS and thus the A cluster will grow at the expense of the B cluster. (There is also the possibility that the single empty site has a third NN empty and thus two B particles can be deposited, but this is a secondary low probability step which requires synergy of three sites.)

V. CONCLUSIONS

In conclusion, we have shown that when a system undergoes a lattice phase transition as a result of high or low level occupation of one (or more) species, spontaneous spatiotemporal oscillations of the species concentrations and clustering of homologous species are induced for specific parameter zones. This has been demonstrated in the case of the Ziff-Gulari-Barshad model of the monomer-dimer process for the R parameter zone $0.3481\leqslant k_1<0.3930$. The method used is kinetic Monte Carlo simulations with direct surface reconstruction from hex$\leftrightarrow$sq lattices. During the reconstruction only the number of nearest neighbors changes while the kinetic parameters remain the same in the two phases (are phase independent).

When the system size is small enough and the transitions take place simultaneously over the entire lattice, the oscilla-

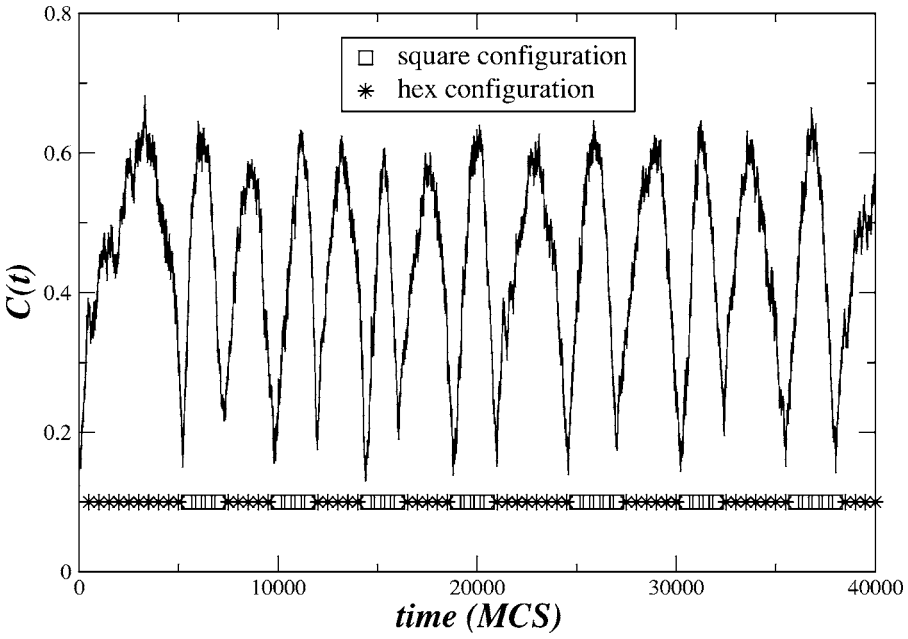

FIG. 5. The covariance function $C(t)$ corresponding to the oscillatory behavior in Fig. 3. The stars (squares) denote the time windows when the system is in the hex (square) configuration.

tions have rather regular shapes with fluctuations as in Figs. 3 and 5. Further KMC simulations have shown that for larger systems with phase transitions taking place locally, the oscillations are irregular and/or chaotic with their synchronization depending on the ratio of the average local reconstructed area to the total lattice size [24]. This type of irregular oscillation is more appropriate for describing experimental situations where the substrates have macroscopic sizes as in the case of heterogeneously catalyzed reactions.

Concerning diffusion, which is important in particular for CO (A) particles at high temperatures, preliminary KMC studies have demonstrated quantitative shifts in the transition points (for example, the abrupt transition in hex configuration shifts from $k_1=0.382$ to 0.384) and thus oscillatory behavior is supported but the width and position of the R region are modified accordingly. Further studies in this direction, using *local* surface reconstruction, surface diffusion, CO and O desorption rates, surface metal oxide formation, and other microscopic known processes are expected to give a better understanding of the complex spatiotemporal structures observed experimentally in heterogeneous catalytic reactions.

ACKNOWLEDGMENTS

V.K.N. acknowledges financial support through the NCSR "Demokritos" program. The authors would like to thank Dr. G. A. Tsekouras and Professor G. Nicolis and Professor A. S. Mikhailov for helpful discussions and suggestions.

[1] G. Ertl, P. R. Norton, and J. Rustig, Phys. Rev. Lett. **49**, 177 (1982); G. Ertl, Science **254**, 1750 (1991).
[2] J. Wintterlin, S. Völkening, T. V. W. Janssens, T. Zambelli, and G. Ertl, Science **278**, 1931 (1997); J. Wintterlin, Adv. Catal. **45**, 131 (2000).
[3] M. Ehsasi, M. Matloch, O. Frank, J. H. Block, K. Christmann, F. S. Rys, and W. Hirschwald, J. Chem. Phys. **91**, 4949 (1989).
[4] R. Imbihl and G. Ertl, Chem. Rev. (Washington, D.C.) **95**, 697 (1995).
[5] S. Y. Shvartsman, E. Schutz, R. Imbihl, and I. G. Kevrekidis, Phys. Rev. Lett. **83**, 2857 (1999).
[6] C. Voss and N. Kruse, Ultramicroscopy **73**, 211 (1998).
[7] N. Hartmann and R. J. Madix, Surf. Sci. **516**, 230 (2002).
[8] B. L. M. Hendriksen and J. W. M. Frenken, Phys. Rev. Lett. **89**, 046101 (2002).
[9] A. S. Mikhailov, Physica A **263**, 329 (1999); K. C. Rose, D. Battogtokh, A. Mikhailov, R. Imbihl, W. Engel, and A. M. Bradshaw, Phys. Rev. Lett. **76**, 3582 (1996).
[10] N. P. Lebedeva, A. Rodes, J. M. Feliu, M. T. M. Koper, and R. A. van Santen, J. Phys. Chem. B **106**, 9863 (2002); N. P. Lebedeva, M. T. M. Koper, J. M. Feliu, and R. A. van Santen, *ibid.* **106**, 12938 (2002).
[11] A. von Oertzen, A. S. Mikhailov, H. H. Rotermundand, and G. Ertl, J. Phys. Chem. B **102**, 4966 (1998); A. von Oertzen, H. H. Rotermundand, A. S. Mikhailov, and G. Ertl, *ibid.* **104**, 3155 (2000).
[12] M. T. M. Koper, A. P. J. Jansen, R. A. van Santen, J. J. Lukkien, and P. A. J. Hilbers, J. Chem. Phys. **109**, 6051 (1998); M. T. M. Koper, J. J. Lukkien, A. P. J. Jansen, and R. A. van Santen, J. Phys. Chem. B **103**, 5522 (1999).
[13] R. F. S. Andrade, G. Dewel, and P. Borckmans, J. Chem. Phys. **91**, 2675 (1989); J. Verdasca, P. Borckmans, and G. Dewel, Phys. Rev. E **64**, 055202 (2001).
[14] R. M. Ziff, E. Gulari, and Y. Barshad, Phys. Rev. Lett. **56**, 2553 (1986); B. J. Brosilow, E. Gulari, and R. M. Ziff, J. Chem. Phys. **98**, 674 (1993); C. A. Voigt and R. M. Ziff, Phys. Rev. E **56**, R6241 (1997).
[15] J. W. Evans, J. Chem. Phys. **98**, 2463 (1993).

[16] D. J. Liu and J. W. Evans, Phys. Rev. Lett. **84**, 955 (2000).
[17] D. J. Liu and J. W. Evans, J. Chem. Phys. **117**, 7319 (2000).
[18] P. A. Carlsson, V. P. Zhdanov, and B. Kasemo, Appl. Surf. Sci. **239**, 424 (2005).
[19] M. D. Graham, M. Bar, I. G. Kevrekidis, K. Asakura, J. Lauterbach, H. H. Rotermund, and G. Ertl, Phys. Rev. E **52**, 76 (1995); J. Wolff, A. G. Papathanasiou, H. H. Rotermund, G. Ertl, M. A. Katsoulakis, X. Li, and I. G. Kevrekidis, Phys. Rev. Lett. **90**, 148301 (2003).
[20] V. P. Zhdanov and B. Kasemo, J. Chem. Phys. **114**, 5351 (2001); V. P. Zhdanov, Surf. Sci. Rep. **45**, 231 (2002).
[21] X. G. Wu and R. Kapral, Physica A **188**, 284 (1992); R. Danielak, A. Perera, M. Moreau, M. Frankowicz, and R. Kapral, *ibid.* **229**, 428 (1996).
[22] O. Kortlüke, V. N. Kuzovkov, and W. von Niessen, Phys. Rev. Lett. **83**, 3089 (1999).
[23] A. Tretyakov, A. Provata, and G. Nicolis, J. Phys. Chem. **99**, 2770 (1995).
[24] G. A. Tsekouras and A. Provata, Phys. Rev. E **65**, 016204 (2002).